

# OTC: A Novel Local Descriptor for Scene Classification

Ran Margolin, Lihi Zelnik-Manor, and Ayellet Tal

Technion Haifa, Israel

**Abstract.** Scene classification is the task of determining the scene type in which a photograph was taken. In this paper we present a novel local descriptor suited for such a task: *Oriented Texture Curves* (OTC). Our descriptor captures the texture of a patch along multiple orientations, while maintaining robustness to illumination changes, geometric distortions and local contrast differences. We show that our descriptor outperforms all state-of-the-art descriptors for scene classification algorithms on the most extensive scene classification benchmark to-date.

**Keywords:** local descriptor, scene classification, scene recognition.

## 1 Introduction

Scene classification addresses the problem of determining the scene type in which a photograph was taken [6,18,21,27] (e.g. kitchen, tennis court, playground). The ability to recognize the scene of a given image can benefit many applications in computer vision, such as content-based image retrieval [32], inferring geographical location from an image [8] and object recognition [22].

Research on scene classification has addressed different parts of the scene classification framework: low-level representations, mid-level representations, high-level representations and learning frameworks.

Works on low-level representations focus on designing an appropriate local descriptor for scene classification. Xiao et al. [34] investigate the benefits of several well known low-level descriptors, such as HOG [2], SIFT [17] and SSIM [26]. Meng et al. [18] suggest the *Local Difference Binary Pattern* (LDBP) descriptor, which can be thought of as an extension of the LBP [20].

Mid-level representations deal with the construction of a global representation from low-level descriptors. Such representations include the well known bag-of-words (BoW) [29] and its extension to the *Spatial Pyramid Matching* (SPM) scheme [13], which by including some spatial considerations, has been shown to provide good results [34,18,13]. Karpac et. al [11] suggest the use of Fisher kernels to encode both the local features as well as their spatial layout.

High-level representations focus on the addition of semantic features [12,31] or incorporating an unsupervised visual concept learning framework [14]. The use of more sophisticated learning frameworks for scene classification include sparse coding [35], hierarchical-learning [27] and deep-learning [4,7].

In this paper, we focus on low-level representations for scene classification. We propose a novel local descriptor: *Oriented Texture Curves* (OTC). The descriptor is based on three key ideas. (i) A patch contains different information along different orientations that should be captured. For each orientation we construct a curve that represents the color variation of the patch along that orientation. (ii) The shapes of these curves characterize the texture of the patch. We represent the shape of a curve by its shape properties, which are robust to illumination differences and geometric distortions of the patch. (iii) Homogeneous patches require special attention to avoid the creation of false features. We do so by suggesting an appropriate normalization scheme. This normalization scheme is generic and can be used in other domains.

Our main contributions are two-fold. First, we propose a novel descriptor, OTC, for scene classification. We show that it achieves an improvement of 7.35% in accuracy over the previously top-performing descriptor, HOG2x2 [5]. Second, we show that a combination between the HOG2x2 descriptor and our OTC descriptor results in an 11.6% improvement in accuracy over the previously top-performing scene classification feature-based algorithm that employs 14 descriptors [34].

## 2 The OTC Descriptor

Our goal is to design a descriptor that satisfies the following two attributes that were shown to be beneficial for scene classification [34].

- **Rotational-Sensitivity:** Descriptors that are not rotationally invariant provide better classification than rotationally invariant descriptors [34]. This is since scenes are almost exclusively photographed parallel to ground. Therefore, horizontal features, such as railings, should be differentiated from vertical features, such as fences. This is the reason why descriptors, such as HOG2x2 [5] and Dense SIFT [13], outperform rotationally invariant descriptors, such as Sparse SIFT [30] and LBP [20,1].
- **Texture:** The top-ranking descriptors for scene classification are texture-based [34]. Furthermore, a good texture-based descriptor should be robust to illumination changes, local contrast differences and geometric distortions [19]. This is since, while different photographs of a common scene may differ in color, illumination or spatial layout, they usually share similar, but not identical, dominant textures. Thus, the HOG2x2 [5], a texture-based descriptor, was found to outperform all other non-texture based descriptors [34].

In what follows we describe in detail the OTC descriptor, which is based on our three key ideas and the two desired attributes listed above. In Section 2.1, we suggest a rotationally-sensitive patch representation by way of multiple curves. The curves characterize the information contained along different orientations of a patch. In Section 2.2 we propose a novel curve representation that is robust

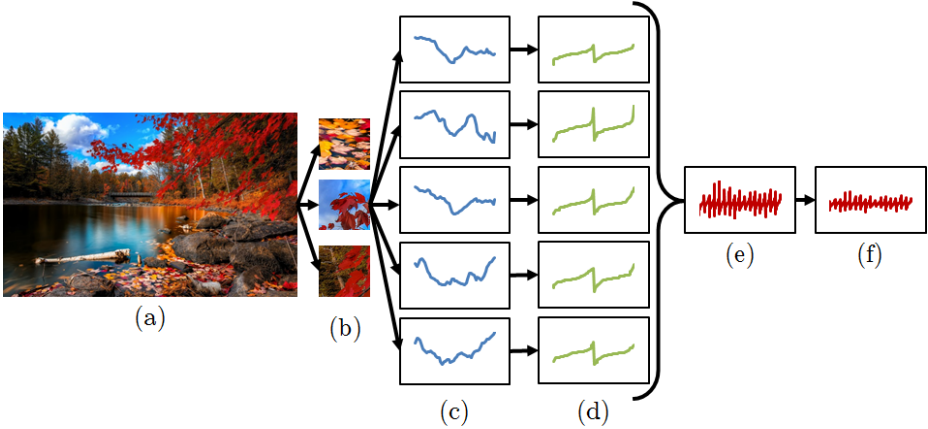


**Fig. 1. OTC overview:** Given an image (a), patches are sampled along a dense grid (b). By traversing each patch along multiple orientations, the patch is represented by multiple curves (c). Each curve is characterized by a novel curve descriptor that is robust to illumination differences and geometric distortions (d). The curve descriptor are then concatenated to form a single descriptor (e). Finally, the OTC descriptor is obtained by applying a novel normalization scheme that avoids the creation of false features while offering robustness to local contrast differences (f).

to illumination differences and geometric distortions. Lastly, we concatenate the obtained multiple curve descriptors into a single descriptor and suggest a novel normalization scheme that avoids the creation of false features in the descriptors of homogeneous patches (Section 2.3). An overview of our framework is illustrated in Figure 1.

## 2.1 Patch to Multiple Curves

Our first goal is to describe the texture of a given patch. It has been shown that different features exhibit different dominant orientations [19]. Thus, by examining a patch along different orientations, different features can be captured.

To do so, we divide an  $N \times N$  patch  $P$  into  $N$  strips along different orientations (in practice, 8), as shown in Figure 2. For each orientation  $\theta$ , an  $N$ -point sampled curve  $c_\theta$  is constructed. The  $i^{\text{th}}$  sampled point along the oriented curve  $c_\theta$  is computed as the mean value of its  $i^{\text{th}}$  oriented strip  $S_{\theta,i}$ :

$$c_\theta(i) = \frac{1}{|S_{\theta,i}|} \sum_{x \in S_{\theta,i}} P(x) \quad 1 \leq i \leq N, \quad (1)$$

$|S_{\theta,i}|$  denoting the number of pixels contained within strip  $S_{\theta,i}$ . For an RGB colored patch,  $C_\theta(i)$  is computed as the mean RGB triplet of its  $i^{\text{th}}$  oriented strip  $S_{\theta,i}$ . Note that by employing strips of predefined orientations, regardless of the input patch, we effectively enforce the desired property of rotational-sensitivity.

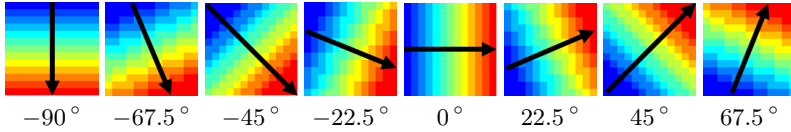


**Fig. 2. Patch to multiple curves:** To represent a patch by multiple curves, we divide the patch into strips (illustrated above as colored strips) along multiple orientations. For each orientation, we construct a curve by first “walking” across the strips (i.e. along the marked black arrows). Then, each point of the curve is defined as the mean value of its corresponding strip.

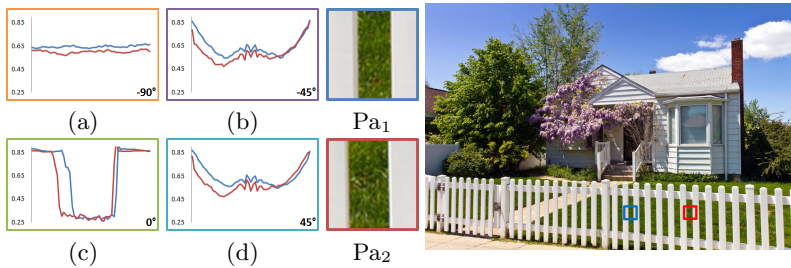


**Fig. 3. Illumination differences and geometric distortions:** (a-d) Curves obtained along four orientations of two very similar patches,  $Pa_1$  &  $Pa_2$  (blue for  $Pa_1$  and red for  $Pa_2$ ). The generated curves are different due to illumination and geometric differences between the patches. Thus, a more robust curve representation is required.

## 2.2 Curve Descriptor

Our second goal is to construct a discriminative descriptor that is robust to illumination differences and geometric distortions. An example why such robustness is needed is presented in Figure 3. Two patches were selected. The patches are very similar but not identical. Differences between them include their illumination, the texture of the grass, the spacing between the white fence posts, and their centering. This can be seen by observing their four curves (generated along four orientations) shown on the left. The differences in illumination can be observed by the difference in heights of the two curves (i.e. the more illuminated patch  $Pa_1$  results in a higher curve than  $Pa_2$ ). The geometric differences between the two patches can be observed in Figure 3(c). Due to the difference in spacing between the white fence posts, the drop of the red curve is to the left of the drop of the blue curve. We hence conclude that these curves are not sufficiently robust to illumination differences and geometric distortions.

Looking again at Figure 3, it can be seen that while the curves are different, their *shapes* are highly similar. To capture the shape of these curves we describe each curve by its gradients and curvatures. For a gray-level patch, for each curve  $c_\theta$  we compute its forward gradient  $c'_\theta(i)$  and an approximation of its curvature  $c''_\theta(i)$  [3] as:

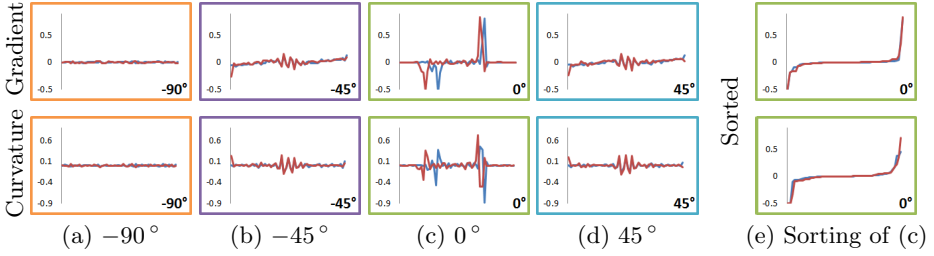


**Fig. 4. Gradients and Curvatures:** The resulting gradients and curvatures of the four curves in Figure 3 (a-d). While offering an improvement in terms of robustness to illumination differences, this representation is still sensitive to geometric distortions (c). By applying a sorting permutation, robustness to such distortions is enforced (e).

$$c'_\theta(i) = c_\theta(i + 1) - c_\theta(i) \quad 1 \leq i < N \quad (2)$$

$$c''_\theta(i) = c'_\theta(i + 1) - c'_\theta(i) \quad 1 \leq i < (N - 1). \quad (3)$$

For RGB curves, we define the forward RGB gradient between two points as the  $L_2$  distance between them, signed according to their gray-level gradient:

$$C'_\theta(i) = \text{sign} \{c'_\theta(i)\} \cdot \|C_\theta(i + 1) - C_\theta(i)\|_2 \quad 1 \leq i < N \quad (4)$$

$$C''_\theta(i) = C'_\theta(i + 1) - C'_\theta(i) \quad 1 \leq i < (N - 1). \quad (5)$$

The resulting gradients and curvatures of the four curves shown in Figure 3 are presented in Figure 4(a-d). While offering an improvement in robustness to illumination differences, the gradients and curvatures in Figure 4(c) still differ. The differences are due to geometric differences between the patches (e.g. the centering of the patch and the spacing between the fence posts). Since scenes of the same category share similar, but not necessarily identical textures, we must allow some degree of robustness to these types of geometric distortions.

A possible solution to this could be some complex distance measure between signals such as dynamic time warping [24]. Apart from the computational penalty involved in such a solution, employing popular mid-level representations such as BoW via K-means is problematic when the centroids of samples are ill-defined. Another solution that has been shown to provide good results are histograms [2,10,17]. While histogram-based representations perform well [19], they suffer from two inherent flaws. The first is quantization error, which may be alleviated to some degree with the use of soft-binning. The second flaw concerns weighted histograms, in which two different distributions may result in identical representations.

Instead, we suggest an alternative orderless representation to that of histograms, which involves applying some permutation  $\pi$  to each descriptor  $C'_\theta$  and  $C''_\theta$ . Let  $\text{dsc}_1$  and  $\text{dsc}_2$  denote two descriptors (e.g. those presented in Figure 4(c)-top in red and blue). The permutation we seek is the one that minimizes the  $L_1$  distance between them:

$$\pi = \arg \min_{\hat{\pi}} \{ \|\hat{\pi}(\text{dsc}_1) - \hat{\pi}(\text{dsc}_2)\|_1 \}. \quad (6)$$

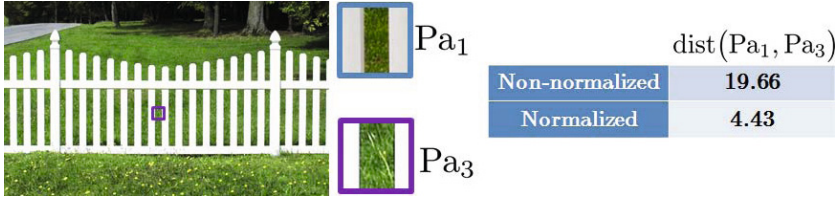


**Fig. 5. Robustness to local contrast differences:** We desire robustness to local contrast differences, such as those present between Pa<sub>1</sub> (from Figure 3) and Pa<sub>3</sub>. By applying a normalization scheme, robustness to such differences is obtained.

A solution to Equation (6) is found in the following theorem, for which we provide proof in Appendix A.

**Theorem 1.** *The permutation that minimizes the  $L_1$  distance between two vectors (descriptors) is the sorting permutation  $\pi_{\text{sort}}$ .*

That is to say, we sort each gradient (or curvature) in a non-decreasing manner. Sorting has been previously used to achieve rotational invariance [33,16]. Yet, since our curves are constructed along predefined orientations, we maintain the desired attribute of rotational-sensitivity, while achieving robustness to geometric distortions. Figure 4(e) illustrates the result of sorting the gradients and curvatures shown in Figure 4(c). It is easy to see that this results in a very similar response for both patches.

### 2.3 H-bin Normalization

Thus far, we have constructed a robust curve representation. Keeping in mind our goal of a patch descriptor, we proceed to concatenate the sorted gradients and curvatures:

$$\text{OTC}_{\text{No-Norm}} = \{\pi_{\text{sort}}(C'_{\theta_1}), \pi_{\text{sort}}(C''_{\theta_1}), \dots, \pi_{\text{sort}}(C'_{\theta_8}), \pi_{\text{sort}}(C''_{\theta_8})\}. \quad (7)$$

While offering a patch descriptor that is robust to illumination differences and geometric distortions, the descriptor still lacks robustness to local contrast differences. An example of such differences is illustrated in Figure 5. A similar patch to that sampled in Figure 3 is sampled from a different image. The patches differ in their local contrast, therefore they are found to have a large  $L_1$  distance.

To support robustness to local contrast differences, we wish to normalize our descriptor. The importance of an appropriate normalization scheme has been previously stressed [2]. Examples of normalization schemes include the well known  $L_1$  and  $L_2$  norms, the overlapping normalization scheme [2] and the  $L_2$ -Hys normalization [17]. Unfortunately, these schemes fail to address the case of a *textureless* patch. Since the OTC descriptor is texture-based, textureless patches result in a descriptor that contains mostly noise. Examples of such patches can be found in the sky region in Figure 3.

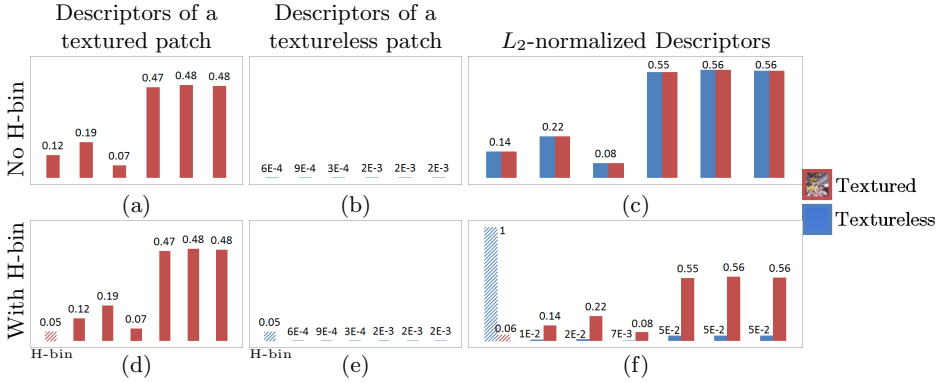


**Fig. 6. H-bin normalization scheme:** Under previous normalization schemes, descriptors of textureless patches (b) are stretched into false features (c)-blue. By adding a low-valued bin, prior to normalization (d-e), false features are avoided (f)-blue. In case of a descriptor of a textured patch (d), the small value hardly affects the normalized result ((f)-red compared to (c)-red). The added H-bin may be thought of as a measure of homogeneity.

The problem of normalizing a descriptor of a textureless patch is that its noisy content is stretched into false features. An example of this can be seen in Figure 6. The descriptors of a textured patch and a textureless patch are shown in Figure 6(a-b). Applying  $L_2$  normalization to both descriptors results in identical descriptors (Figure 6(c)).

To overcome this, we suggest a simple yet effective method. For each descriptor, we add a small-valued bin (0.05), which we denote as the *Homogeneous-bin* (H-bin). While the rest of the descriptor measures the features within a patch, the H-bin measures the lack of features therein. We then apply  $L_2$  normalization. Due to the small value of the H-bin, it hardly affects patches that contain features. Yet, it prevents the generation of false features in textureless patches. An example can be seen in Figure 6. An H-bin was added to the descriptor of both textured and textureless patches (Figure 6(d-e)). After normalization, the descriptor of the textured patch is hardly affected ((f)-red compared to (c)-red). Yet, the normalized descriptor of the textureless patch retains its low valued features. This is while indicating the presence of a textureless patch by its large H-bin (Figure 6(f)-blue). In Figure 7(b) we present the H-bins of the  $L_2$ -normalized OTC descriptors of Figure 7(a). As expected the sky region is found as textureless, while the rest of the image is identified as textured.

Thus, the final OTC descriptor is obtained by:

$$OTC = \frac{\{H\text{-bin}, OTC_{No-Norm}\}}{\left\| \left\{ H\text{-bin}, OTC_{No-Norm} \right\} \right\|_2}. \tag{8}$$

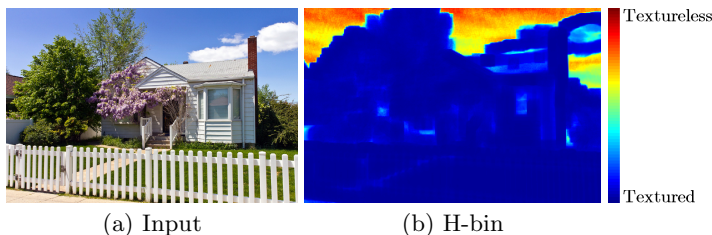


**Fig. 7. H-bin visualization:** (b) The normalized H-bins of the OTC descriptors of (a). As expected, patches with little texture result in a high normalized H-bin value.

### 3 Evaluation

**Benchmark:** To evaluate the benefit of our OTC descriptor, we test its performance on the SUN397 benchmark [34], the most extensive scene classification benchmark to-date. The benchmark includes 397 categories, amounting to a total of 108,574 color images, which is several orders of magnitude larger than previous datasets. The dataset includes a widely diverse set of indoor and outdoor scenes, ranging from elevator-shafts to tree-houses, making it highly robust to over-fitting. In addition, the benchmark is well defined with a strict evaluation scheme of 10 cross-validations of 50 training images and 50 testing images per category. The average accuracy across all categories is reported.

**OTC Setup:** To fairly evaluate the performance of our low-level representation, we adopt the simple mid-level representation and learning scheme that were used in [34]. Given an image, we compute its OTC descriptors on a dense  $3 \times 3$  grid (images were resized to contain no more than  $300^2$  pixels). Each descriptor is computed on a  $13 \times 13$  sized patch, resulting in a total length of  $\underbrace{8}_{\text{orientations}} \times (\underbrace{12}_{\text{gradient}} + \underbrace{11}_{\text{curvature}}) = 184$  values per patch. After adding the H-bin and normalizing, our final descriptors are of length 185. The local OTC descriptors are then used in a 3-level Spatial Pyramid Matching scheme (SPM) [13] with a BoW of 1000 words via  $L_1$  K-means clustering. Histogram intersection [13] is used to compute the distance between two SPMs. Lastly, we use a simple 1-vs-all SVM classification framework.

In what follows we begin by comparing the classification accuracy of our OTC descriptor to state-of-the-art descriptors and algorithms (Section 3.1). We then proceed in Section 3.2 to analyze its classification performance in more detail.

#### 3.1 Benchmark Results

To demonstrate the benefits of our low-level representation we first compare our OTC descriptor to other state-of-the-art low-level descriptors with the common mid-level representation and a 1-vs-all SVM classification scheme of [34].

In Table 1(left) we present the top-four performing descriptors on the SUN397 benchmark [34]: (1) *Dense SIFT* [13]: SIFT descriptors are extracted on a dense

grid for each of the HSV color channels and stacked together. A 3-level SPM mid-level representation with a 300 BoW is used. (2) *SSIM* [26]: SSIM descriptors are extracted on a dense grid and quantized into a 300 BoW. The  $\chi^2$  distance is used to compute the distance between two spatial histograms. (3) *G-tex* [34]: Using the method of [9], the probability of four geometric classes are computed: ground, vertical, porous and sky. Then, a texton histogram is built for each class, weighted by the probability that it belongs to that geometric class. The histograms are normalized and compared with the  $\chi^2$  distance. (4) *HOG2x2* [5]: HOG descriptors are computed on a dense grid. Then,  $2 \times 2$  neighboring HOG descriptors are stacked together to provide enhanced descriptive power. Histogram intersection is used to compute the distance between the obtained 3-level SPMs with a 300 BoW.

As shown in Table 1, our proposed OTC descriptor significantly outperforms previous descriptors. We achieve an improvement of 7.35% with a 1000 BoW and an improvement of 3.98% with a 300 BoW (denoted OTC-300).

**Table 1. SUN397 state-of-the-art performance:** *Left:* Our OTC descriptor outperforms all previous descriptors. *Right:* Performance of more complex state-of-the-art algorithms. Our simple combination of OTC and HOG2x2 outperforms most of the state-of-the-art algorithms.

Descriptors		Algorithms	
Name	Accuracy	Name	Accuracy
Dense SIFT [13]	21.5	ML-DDL [27]	23.1
SSIM [26]	22.5	S-Manifold [12]	28.9
G-tex [34]	23.5	<b>OTC</b>	<b>34.56</b>
HOG2x2 [5]	27.2	contextBow-m+semantic [31]	35.6
OTC-300	31.18	14 Combined Features [34]	38
<b>OTC</b>	<b>34.56</b>	DeCAF [4]	40.94
		<b>OTC + HOG2x2</b>	<b>49.6</b>
		MOP-CNN [7]	51.98

Since most recent works deal with mid-level representations, high-level representations and learning schemes, we further compare in Table 1(right) our descriptor to more complex state-of-the-art scene classification algorithms: (1) *ML-DDL* [27] suggests a novel learning scheme that takes advantage of the hierarchical correlation between scene categories. Based on densely sampled SIFT descriptors a dictionary and a classification model are learned for each hierarchy (3 hierarchies are defined for the SUN397 dataset [34]). (2) *S-Manifold* [12] suggests a mid-level representation that combines the SPM representation with a semantic manifold [25]. Densely samples SIFT descriptors are used as local descriptors. (3) *contextBoW-m+semantic* [31] suggests both mid-level and high-level representations in which pre-learned context classifiers are used to construct multiple context-based BoWs. Five local features are used (four low-level and one high-level): SIFT, texton filterbanks, LAB color values, Canny edge detection and the inferred semantic classification. (4) *14 Combined Features* [34] combines the distance kernels obtained by 14 descriptors (four of which appear

in Table 1(left)). (5,6) *DeCAF* [4] & *MOP-CNN* [7] both employ a deep convolutional neural network.

In Table 1(right) we show that by simply combining the distance kernels of our OTC descriptor and those of the HOG2x2 descriptor (at a 56-44 ratio), we outperform most other more complex scene classification algorithms. A huge improvement of 11.6% over the previous top performing feature-based algorithm is achieved. A nearly comparable result is achieved when compared to MOP-CNN that is based on a complex convolutional neural network.

For completeness, in Table 2 we compare our OTC descriptor on two additional smaller benchmarks: the 15-scene dataset [13] and the MIT-indoor dataset [23]. In both benchmarks, our simplistic framework outperforms all other descriptors in similar simplistic frameworks. Still, several state-of-the-art complex methods offer better performance than our framework. We believe that incorporating our OTC descriptor into these more complex algorithms would improve their performance even further.

**Table 2. 15-scene & MIT-indoor datasets:** Our OTC descriptor outperforms previous descriptors and is comparable with several more complex methods

15-scene		MIT-indoor	
Name	Accuracy	Name	Accuracy
SSIM [26]	77.2	SIFT [13]	34.40
G-tex [34]	77.8	Discriminative patches [28]	38.10
HOG2x2 [5]	81.0	<b>OTC</b>	<b>47.33</b>
SIFT [13]	81.2	Disc. Patches++ [28]	49.40
<b>OTC</b>	<b>84.37</b>	ISPR + IFV [15]	68.5
ISPR + IFV [15]	91.06	MOP-CNN [7]	68.88

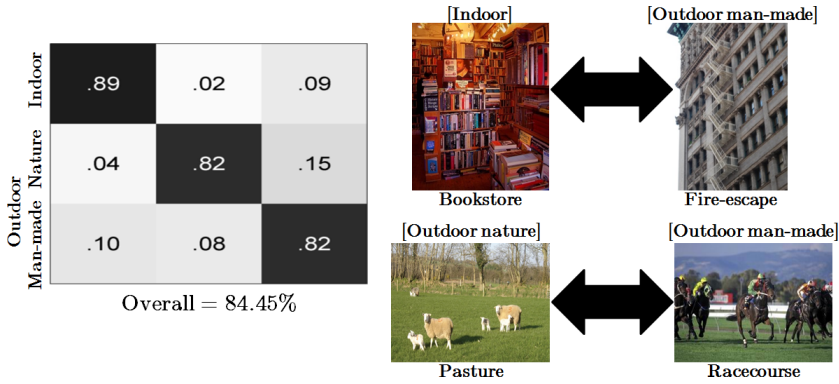
### 3.2 Classification Analysis

In what follows we provide an analysis of the classification accuracy of our descriptor on the top two hierarchies of the SUN397 dataset. The 1<sup>st</sup> level consists of three categories: indoor, outdoor nature and outdoor man-made. The 2<sup>nd</sup> level consists of 16 categories (listed in Figure 9).

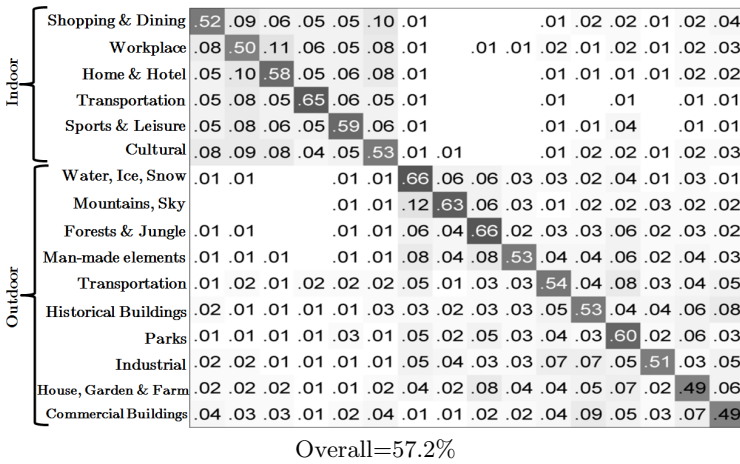
In Figure 8(left) we present the confusion matrix on the 1<sup>st</sup> level of the SUN397 dataset for which an impressive 84.45% success rate is achieved (comparison to other methods is shown later). Studying the matrix, confusion is mostly apparent between indoor & outdoor man-made scenes and within the two types of outdoor scenes. Misclassification between indoor and outdoor man-made scenes is understandable, since both scene types consist of similar textures such as straight horizontal and vertical lines, as evident by comparing the image of the Bookstore scene to that of the Fire-escape (Figure 8(top-right)). Differences between outdoor nature scenes and outdoor man-made scenes are often contextual, such as the Pasture and Racecourse images shown in

Figure 8(bottom-right). Thus, it is no surprise that a texture-based classification may confuse between the two.

The 2<sup>nd</sup> level confusion matrix is displayed in Figure 9. Our average success rate is 57.2%. Most confusions occur between categories of similar indoor or outdoor settings. Furthermore, we note that the two categories with the highest errors are Commercial Buildings and House, Garden & Farm. The former is



**Fig. 8. 1<sup>st</sup> level confusion matrix:** *Left:* The confusion matrix of our OTC descriptor on the 1<sup>st</sup> level of the SUN397 dataset shows that most misclassifications occur between indoor & outdoor man-made scenes, and within the two types of outdoor scenes. *Right:* Images in which the classification was mistakenly swapped.



**Fig. 9. 2<sup>nd</sup> level confusion matrix:** The confusion matrix of our OTC descriptor on the 2<sup>nd</sup> level of the SUN397 dataset shows that most confusions occur between categories of similar indoor or outdoor settings. Furthermore, most confusions occur between classes of semantic differences such as Home & Hotel and Workplace. These understandable misclassifications further confirm the strength of our OTC descriptor at capturing similar textures.

mostly confused with Historical Buildings and the latter with Forests & Jungle. These understandable semantic confusions further confirm the robustness of the classification strength of our OTC descriptor.

Lastly, we compare in Table 3 the average classification accuracy of our OTC descriptor on each of the three hierarchical levels, to that of ML-DDL [27]. ML-DDL is the best performing algorithm to reports results on the different hierarchies. In all three levels our descriptor outperforms the results of ML-DDL, which utilizes a hierarchical based learning framework.

**Table 3. SUN397 hierarchical classification:** Our OTC descriptor outperforms the hierarchical based learning framework of [27] on all of the three hierarchical levels of the SUN397 dataset

Name	Accuracy		
	1 <sup>st</sup>	2 <sup>nd</sup>	3 <sup>d</sup>
ML-DDL [27]	83.4	51	23.1
<b>OTC</b>	<b>84.45</b>	<b>57.2</b>	<b>34.56</b>

## 4 Conclusion

We presented the OTC descriptor, a novel low-level representation for scene classification. The descriptor is based on three main ideas. First, representing the texture of a patch along different orientations by the shapes of multiple curves. Second, using sorted gradients and curvatures as curve descriptors, which are robust to illumination differences and geometric distortions of the patch. Third, enforcing robustness to local contrast differences by applying a novel normalization scheme that avoids the creation of false features.

Our descriptor achieves an improvement of 7.35% in accuracy over the previously top-performing descriptor, on the most extensive scene classification benchmark [34]. We further showed that a combination between the HOG2x2 descriptor [5] and our OTC descriptor results in an 11.6% improvement in accuracy over the previously top-performing scene classification feature-based algorithm that employs 14 descriptors.

## A Proof of Theorem 1

**Theorem 1.** *The permutation that minimizes the  $L_1$  distance between two vectors (descriptors) is the sorting permutation  $\pi_{\text{sort}}$ .*

*Proof.* Let  $\hat{a}_{1 \times N}$  and  $\hat{b}_{1 \times N}$  be two vectors of length  $N$ . We apply permutation  $\pi_b$  that sorts the elements of  $\hat{b}_{1 \times N}$  to both vectors  $\hat{a}_{1 \times N}$  and  $\hat{b}_{1 \times N}$ . Note that applying this permutation to both vectors ( $a_{1 \times N} = \pi_b(\hat{a}_{1 \times N}), b_{1 \times N} = \pi_b(\hat{b}_{1 \times N})$ )

does not change their  $L_1$  distance.

Proof by induction on the length of the vectors,  $N$ :

For the basis of the induction let  $N = 2$ . Let  $x_i$  denote the  $i^{th}$  element in vector  $x$ . Below we provide proof for the case of  $a_1 \leq a_2$  (Recall that  $b_1 \leq b_2$ ). A similar proof can be done for  $a_2 \leq a_1$ .

We show that  $\underbrace{|b_1 - a_1| + |b_2 - a_2|}_{LH} \leq \underbrace{|b_1 - a_2| + |b_2 - a_1|}_{RH}$ :

$$(b_1 \leq b_2 \leq a_1 \leq a_2): LH = a_1 + a_2 - b_1 - b_2 = RH \tag{9}$$

$$(b_1 \leq a_1 \leq b_2 \leq a_2): LH = a_1 - b_2 + a_2 - b_1 \underset{a_1 \leq b_2}{\leq} = b_2 - a_1 + a_2 - b_1 = RH \tag{10}$$

$$(b_1 \leq a_1 \leq a_2 \leq b_2): LH = a_1 - b_1 + b_2 - a_2 \underset{a_1 \leq a_2}{\leq} = a_2 - b_1 + b_2 - a_1 = RH \tag{11}$$

$$(a_1 \leq b_1 \leq b_2 \leq a_2): LH = b_1 - a_1 + a_2 - b_2 \underset{b_1 \leq b_2}{\leq} = b_2 - a_1 + a_2 - b_1 = RH \tag{12}$$

$$(a_1 \leq b_1 \leq a_2 \leq b_2): LH = b_1 - a_1 + b_2 - a_2 \underset{b_1 \leq a_2}{\leq} = a_2 - a_1 + b_2 - b_1 = RH \tag{13}$$

$$(a_1 \leq a_2 \leq b_1 \leq b_2): LH = b_1 + b_2 - a_1 - a_2 = RH \tag{14}$$

Now suppose that the theorem holds for  $N < K$ . We prove that it holds for  $N = K$ .

First, we prove that given a permutation  $\pi$  that minimizes  $\|b - \pi(a)\|_1 \Rightarrow \pi$  is the sorting permutation  $\pi_{sort}$ .

Let  $\pi$  be some permutation applied to  $a$ , so that a minimal  $L_1$  distance is achieved:

$$\pi = \arg \min_{\pi} \{ \|b - \pi(a)\|_1 \}. \tag{15}$$

Let  $x_{i:j}$  denote a sub-vector of a vector  $x$  from index  $i$  to index  $j$ .

We can decompose  $D = \|b - \pi(a)\|_1$  into  $D = \underbrace{\|b_1 - \pi(a)_1\|_1}_{D_1} + \underbrace{\|b_{2:K} - \pi(a)_{2:K}\|_1}_{D_{2:K}}$ .

The minimality of  $D$  infers the minimality of  $D_{2:K}$ . Otherwise, a smaller  $L_1$  distance can be found by reordering the elements of  $\pi(a)_{2:K}$ , contradicting the minimality of  $D$ . Following our hypothesis, we deduce that  $\pi(a)_{2:K}$  is sorted. Specifically  $\pi(a)_2 = \min\{\pi(a)_{2:K}\}$ .

Similarly, by decomposing  $D$  into  $D = \underbrace{\|b_{1:(K-1)} - \pi(a)_{1:(K-1)}\|_1}_{D_{1:(K-1)}} + \underbrace{\|b_K - \pi(a)_K\|_1}_{D_K}$

we deduce that  $\pi(a)_1 = \min\{\pi(a)_{1:(K-1)}\} \leq \pi(a)_2$ .

This implies, that  $\pi(a)$  is sorted and that  $\pi = \pi_{sort}$ .

Next, we prove the other side, i.e. if  $\pi = \pi_{sort} \Rightarrow \pi$  minimizes  $\|b - \pi(a)\|_1$ .

Assume to the contrary that there exists a non-sorting permutation  $\pi_{min} \neq \pi_{sort}$

that can achieve a minimal  $L_1$  distance  $D'$ , which is smaller than  $D = \|b - \pi_{sort}(a)\|_1$ . Then, there must be at least two elements  $\pi_{min}(a)_i > \pi_{min}(a)_j$  that are out of order (i.e.  $i < j$ ).

We can decompose  $D'$  into:

$$D' = \sum_{k \neq i, j} |b_k - \pi_{min}(a)_k| + \|(b_i, b_j) - (\pi_{min}(a)_i, \pi_{min}(a)_j)\|_1. \quad (16)$$

$$(17)$$

Yet, as proved in the basis of our induction, the following inequality is true:

$$\|(b_i, b_j) - (\pi_{min}(a)_i, \pi_{min}(a)_j)\|_1 \underbrace{\leq}_{\pi_{min}(a)_j < \pi_{min}(a)_i} \|(b_i, b_j) - (\pi_{min}(a)_j, \pi_{min}(a)_i)\|_1. \quad (18)$$

Therefore, a smaller  $L_1$  distance can be achieved (by reordering  $\pi_{min}(a)_i$  and  $\pi_{min}(a)_j$ ), contradicting the assumption that  $D'$  is minimal. Thus, no other permutation can achieve a smaller  $L_1$  distance than the sorting permutation (i.e.  $\pi_{sort}$  is the permutation that minimizes  $\|b - \pi_{sort}(a)\|_1$ ).  $\square$

## References

1. Ahonen, T., Matas, J., He, C., Pietikäinen, M.: Rotation invariant image description with local binary pattern histogram fourier features. In: Salberg, A.-B., Hardeberg, J.Y., Jenssen, R. (eds.) SCIA 2009. LNCS, vol. 5575, pp. 61–70. Springer, Heidelberg (2009)
2. Dalal, N., Triggs, B.: Histograms of oriented gradients for human detection. In: CVPR, vol. 1, pp. 886–893 (2005)
3. Do, C., Manfredo, P.: Differential geometry of curves and surfaces, vol. 2. Prentice-Hall Englewood Cliffs (1976)
4. Donahue, J., Jia, Y., Vinyals, O., Hoffman, J., Zhang, N., Tzeng, E., Darrell, T.: Decaf: A deep convolutional activation feature for generic visual recognition. In: International Conference on Machine Learning, pp. 647–655 (2014)
5. Felzenszwalb, P.F., Girshick, R.B., McAllester, D., Ramanan, D.: Object detection with discriminatively trained part-based models. PAMI 32(9), 1627–1645 (2010)
6. Gao, T., Koller, D.: Discriminative learning of relaxed hierarchy for large-scale visual recognition. In: ICCV, pp. 2072–2079 (2011)
7. Gong, Y., Wang, L., Guo, R., Lazebnik, S.: Multi-scale orderless pooling of deep convolutional activation features. CoRR (2014)
8. Hays, J., Efros, A.A.: Im2gps: estimating geographic information from a single image. In: CVPR, pp. 1–8 (2008)
9. Hoiem, D., Efros, A.A., Hebert, M.: Recovering surface layout from an image. IJCV 75(1), 151–172 (2007)
10. Koenderink, J.J., Van Doorn, A.J.: The structure of locally orderless images. IJCV 31(2-3), 159–168 (1999)
11. Krapac, J., Verbeek, J., Jurie, F.: Modeling spatial layout with fisher vectors for image categorization. In: ICCV, pp. 1487–1494 (2011)
12. Kwitt, R., Vasconcelos, N., Rasiwasia, N.: Scene recognition on the semantic manifold. In: Fitzgibbon, A., Lazebnik, S., Perona, P., Sato, Y., Schmid, C. (eds.) ECCV 2012, Part IV. LNCS, vol. 7575, pp. 359–372. Springer, Heidelberg (2012)

13. Lazebnik, S., Schmid, C., Ponce, J.: Beyond bags of features: Spatial pyramid matching for recognizing natural scene categories. In: CVPR, pp. 2169–2178 (2006)
14. Li, Q., Wu, J., Tu, Z.: Harvesting mid-level visual concepts from large-scale internet images. In: CVPR, pp. 851–858 (2013)
15. Lin, D., Lu, C., Liao, R., Jia, J.: Learning important spatial pooling regions for scene classification. In: CVPR (2014)
16. Liu, L., Fieguth, P., Kuang, G., Zha, H.: Sorted random projections for robust texture classification. In: ICCV, pp. 391–398 (2011)
17. Lowe, D.G.: Object recognition from local scale-invariant features. In: ICCV, vol. 2, pp. 1150–1157 (1999)
18. Meng, X., Wang, Z., Wu, L.: Building global image features for scene recognition. *Pattern Recognition* 45(1), 373–380 (2012)
19. Mikolajczyk, K., Schmid, C.: A performance evaluation of local descriptors. *PAMI* 27(10), 1615–1630 (2005)
20. Ojala, T., Pietikainen, M., Maenpaa, T.: Multiresolution gray-scale and rotation invariant texture classification with local binary patterns. *PAMI* 24(7), 971–987 (2002)
21. Oliva, A., Torralba, A.: Modeling the shape of the scene: A holistic representation of the spatial envelope. *IJCV* 42(3), 145–175 (2001)
22. Oliva, A., Torralba, A.: The role of context in object recognition. *Trends in Cognitive Sciences* 11(12), 520–527 (2007)
23. Quattoni, A., Torralba, A.: Recognizing indoor scenes. In: CVPR (2009)
24. Rabiner, L.R., Juang, B.H.: *Fundamentals of speech recognition*. Prentice Hall (1993)
25. Rasiwasia, N., Vasconcelos, N.: Scene classification with low-dimensional semantic spaces and weak supervision. In: CVPR, pp. 1–6 (2008)
26. Shechtman, E., Irani, M.: Matching local self-similarities across images and videos. In: CVPR, pp. 1–8 (2007)
27. Shen, L., Wang, S., Sun, G., Jiang, S., Huang, Q.: Multi-level discriminative dictionary learning towards hierarchical visual categorization. In: CVPR, pp. 383–390 (2013)
28. Singh, S., Gupta, A., Efros, A.A.: Unsupervised discovery of mid-level discriminative patches. In: Fitzgibbon, A., Lazebnik, S., Perona, P., Sato, Y., Schmid, C. (eds.) *ECCV 2012, Part II. LNCS*, vol. 7573, pp. 73–86. Springer, Heidelberg (2012)
29. Sivic, J., Zisserman, A.: Video google: A text retrieval approach to object matching in videos. In: ICCV, pp. 1470–1477 (2003)
30. Sivic, J., Zisserman, A.: Video data mining using configurations of viewpoint invariant regions. In: CVPR, p. I-488 (2004)
31. Su, Y., Jurie, F.: Improving image classification using semantic attributes. *IJCV* 100(1), 59–77 (2012)
32. Vogel, J., Schiele, B.: Semantic modeling of natural scenes for content-based image retrieval. *IJCV* 72(2), 133–157 (2007)
33. Wang, Z., Fan, B., Wu, F.: Local intensity order pattern for feature description. In: ICCV, pp. 603–610 (2011)
34. Xiao, J., Hays, J., Ehinger, K.A., Oliva, A., Torralba, A.: Sun database: Large-scale scene recognition from abbey to zoo. In: CVPR, pp. 3485–3492 (2010)
35. Yang, J., Yu, K., Gong, Y., Huang, T.: Linear spatial pyramid matching using sparse coding for image classification. In: CVPR, pp. 1794–1801 (2009)